Plant Cell Physiol. 49(9): 1350–1363 (2008)
doi:10.1093/pcp/pcn111, available online at www.pcp.oxfordjournals.org

Role of *Arabidopsis* CHL27 Protein for Photosynthesis, Chloroplast Development and Gene Expression Profiling

Woo Young Bang [1,3], In Sil Jeong [1,3], Dae Won Kim [1], Chak Han Im [1], Chen Ji [1], Sung Min Hwang [1], Se Won Kim [1], Young Sim Son [1], Joa Jeong [1], Takashi Shiina [2] and Jeong Dong Bahk [1,*]

[1] *Division of Applied Life Sciences (BK21-EBNCRC), Graduate School of Gyeongsang National University, Jinju 660-701, Korea*
[2] *Graduate School of Human and Environmental Sciences, Kyoto Prefectural University, Shimogamo, Sakyo-ku, Kyoto, 606-8522 Japan*

In Chl biosynthesis, aerobic Mg-protoporphyrin IX monomethyl ester (MPE) cyclase is a key enzyme involved in the synthesis of protochlorophyllide *a*, and its membrane-bound component is known to be encoded by homologs of *CHL27* in photosynthetic bacteria, green algae and plants. Here, we report that the *Arabidopsis chl27-t* knock-down mutant exhibits retarded growth and chloroplast developmental defects that are caused by damage to PSII reaction centers. The mutant contains a T-DNA insertion within the *CHL27* promoter that dramatically reduces the *CHL27* mRNA level. *chl27-t* mutant plants grew slowly with a pale green appearance, suggesting that they are defective in Chl biosynthesis. Chl fluorescence analysis showed significantly low photosynthetic activity in *chl27-t* mutants, indicating damage in their PSII reaction centers. The *chl27-t* mutation also conferred severe defects in chloroplast development, including the unstacking of thylakoid membranes. Microarray analysis of the *chl27-t* mutant showed repression of numerous nuclear genes involved in photosynthesis, including those encoding components of light-harvesting complex I (LHCI) and LHCII, and PSI and PSII, which accounts for the defects in photosynthetic activity and chloroplast development. In addition, the microarray data also revealed the significant repression of genes such as *PORA* and *AtFRO6* for Chl biosynthesis and iron acquisition, respectively, and, furthermore, implied that there is cross-talk in the Chl biosynthetic pathway among the PORA, AtFRO6 and CHL27 proteins.

Keywords: AtFRO6 — *chl27-t* mutant — Chloroplast development — Microarray analysis — PORA— PSII.

Abbreviations: CAO, chlorophyllide *a* oxygenase; ETR, relative electron transport rate; FRO, ferric chelate reductase; GFP, green fluorescent protein; LHC, light-harvesting complex; MPE, Mg-protoporphyrin IX monomethyl ester; MS, Murashige and Skoog; NPQ, non-photochemical quenching; PAM, pulse amplitude modulation; PAR, photosynthetically active radiation; POR, NADPH-protochlorophyllide oxidoreductase; RFP, red fluorescent protein; RT–PCR, reverse transcription–PCR; 5′-UTR, 5′-untranslated region.

Introduction

Chls are essential pigments that trap light energy in the antenna system and transfer the energy to reaction centers (Buchanan et al. 2000), and they also have a potential role in chloroplast development (Eckhardt et al. 2004). Chl molecules are produced in a biosynthetic pathway with numerous catalytic enzymes responsible for the production of various intermediates (Chew and Bryant 2007, Tanaka and Tanaka 2007). The Chl biosynthetic pathway begins with the condensation of 5-aminolevulinic acid to uroporphyrinogen III, the first closed tetrapyrrole. Uroporphyrinogen III is subsequently converted to protoporphyrin IX, which is a common intermediate in heme and Chl synthesis. For Chl production, a magnesium ion is inserted into protoporphyrin IX by magnesium chelatase, resulting in the formation of Mg-protoporphyrin IX, which is converted to Mg-protoporphyrin IX monomethyl ester (MPE) by a methyl transferase. In the next step, an MPE cyclase catalyzes the conversion of MPE to protochlorophyllide *a* by making an isocyclic ring (fifth ring), a characteristic of all Chls and bacteriochlorophylls. In angiosperms, the protochlorophyllide is converted in a light-dependent manner to chlorophyllide *a* by NADPH-protochlorophyllide oxidoreductase (POR), and finally, a polyisoprene tail is added to complete Chl *a*, which can be converted to Chl *b* via the activity of chlorophyllide *a* oxygenase (CAO) in land plants.

For producing protochlorophyllide *a* under aerobiosis, green algae and plants use an aerobic MPE cyclase, identified originally as the *acsF* gene in *Rubrivivax gelatinosus*, a photosynthetic bacterium (Pinta et al. 2002). Subsequently, homologs of *AcsF* such as *PNZIP*, *Crd1*, *CHL27* and *Xantha-l* were also identified as aerobic MPE cyclases containing a consensus carboxylate-bridged

[3]These authors contributed equally to this work.
*Corresponding author: E-mail, jdbahk@gnu.ac.kr; Fax, +82-55-752-7062.

di-iron-binding site (Zheng et al. 1998, Moseley et al. 2000, Pinta et al. 2002, Tottey et al. 2003, Rzeznicka et al. 2005). *PNZIP* in *Pharbitis nil* has been found to be regulated by phytochrome and circadian rhythms (Zheng et al. 1998), and *Crd1* in *Chlamydomonas reinhardtii* is required for the accumulation of PSI and light-harvesting complex I (LHCI) during hypoxia or copper deficiency (Moseley et al. 2000). Recently, an in vitro assay for the aerobic cyclase reaction showed that extracts from *xantha-l* and *viridis-k*, two barley mutants, have no cyclase activity, and it was demonstrated that the aerobic cyclase is composed of at least one soluble and two membrane-bound components, and that the *Xantha-l* gene, a homolog of *CHL27*, encodes a membrane-bound subunit of this enzyme complex (Rzeznicka et al. 2005). In addition, Tottey et al. (2003) reported that antisense *Arabidopsis* mutants for the *CHL27* gene have a chlorotic phenotype with the accumulation of MPE as a cyclase reaction substrate, indicating that *CHL27* is required for the synthesis of protochlorophyllide *a*.

Mutants defective in the Chl biosynthetic pathway have been identified in diverse plant species, and their genetic characteristics, physiological phenotypes, chloroplast morphologies and photosynthetic properties have been investigated systematically (Havaux and Tardy 1997, Pontier et al. 2007, Wu et al. 2007). However, the photosynthesis and chloroplast morphology phenotypes conferred by mutations in *CHL27* homologs have not been reported, although a few mutants have been identified in *Arabidopsis* and barely (Tottey et al. 2003, Rzeznicka et al. 2005). In the present work, we identified an *Arabidopsis chl27-t* mutant containing a T-DNA insertion in the promoter region of the *CHL27* gene, which leads to growth retardation, and investigated the mutant with respect to fluorescence parameters and chloroplast morphology. We also analyzed the transcriptome profile of the *chl27-t* mutant using microarray analysis and examined the cause of the photosynthetic and chloroplast developmental defects of the *chl27-t* mutant. In addition, on the basis of our microarray data, we propose that there may be cross-talk in the Chl biosynthetic pathway among the PORA, AtFRO6 and CHL27 proteins.

Results

CHL27 locus organization and transcription in a chl27-t mutant

A mutant with a T-DNA insertion in the *Arabidopsis CHL27* gene was obtained from the Salk Institute Genomic Analysis Laboratory collection, and its inserted portion was confirmed by searching the insertion flanking sequence database using the *CHL27* cDNA as a query sequence (Alonso et al. 2003). PCR genotyping analysis allowed the selection of homozygous mutant plants, and sequence analysis confirmed a T-DNA insertion in the promoter region of *CHL27*, 101 bases upstream of the translation start site (Fig. 1A). Moreover, RNA gel blot analysis using a *CHL27*-specific probe showed a significantly reduced level of *CHL27* mRNA and showed that *CHL27* was expressed with a 24 h periodicity in both mutant and wild-type plants (Fig. 1B, C), similar to the circadian expression of *PNZIP*, a *CHL27* homolog in *P. nil* (Zheng et al. 1998). From reverse transcription–PCR (RT–PCR) and microarray

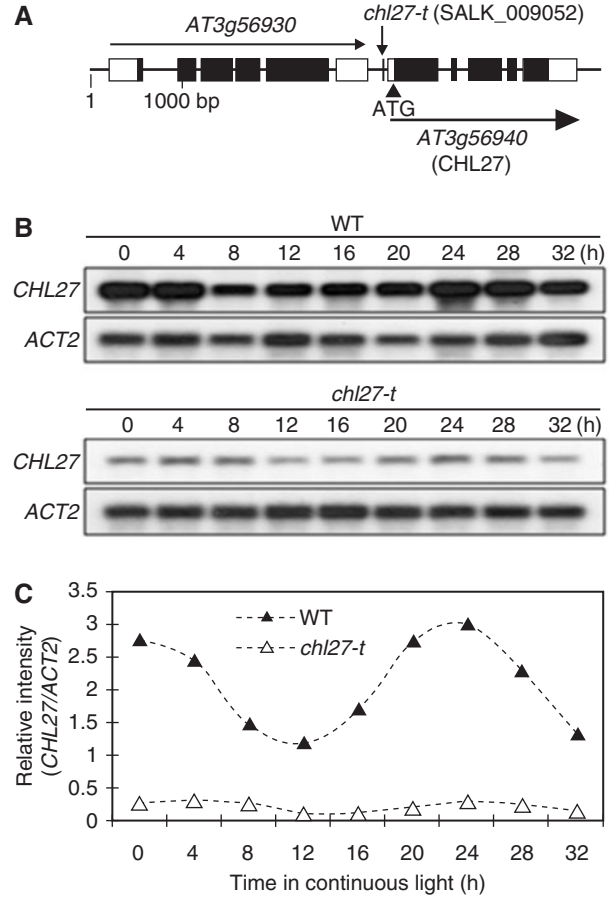

Fig. 1 *CHL27* locus organization and transcription level in the *chl27-t* mutant. (A) Schematic drawing of the At3g56940 locus encoding the CHL27 (NP_191253) protein, and structure of the *chl27-t* allele (SALK_009052) identified in a T-DNA insertion population. Open and filled boxes indicate exons encoding UTRs and protein-coding regions, respectively. A T-DNA is inserted within the promoter region of the annotated At3g56940 (*CHL27*), 101 bases upstream of the translation start site. (B) RNA gel blot analysis of the *CHL27* mRNA level in wild-type and *chl27-t* plants. Wild-type and *chl27-t* seedlings were grown under 12 h light and 12 h darkness for 7 d and then transferred to continuous light. At the time (h) indicated, leaves were harvested and RNA was isolated. Each lane contains 20 μg of total RNA, and *ACT2*, an *Arabidopsis ACTIN2* gene, was used as a control for equal loading of RNA in each lane. (C) Measurement of the *CHL27/ACT2* ratio. The relative intensities of the *CHL27* and *ACT2* bands in B were measured with a GS-700 imaging densitometer.

analysis, we also demonstrated that the expression of the *At3g56930* gene, close to the T-DNA insertion (Fig. 1A), was unaffected in the mutant (Supplementary Fig. S1). These results suggest that the T-DNA insertion in the *CHL27* promoter leads to a reduction in *CHL27* expression but that it has no effect on the circadian regulation of *CHL27*. We named the mutant *chl27-t*, and T_4 plants generated by self-pollination of homozygous T_3 *chl27-t* plants were used for further experiments.

Growth retardation and abnormal phenotypes of the homozygous chl27-t mutant

chl27-t mutant plants grown in Murashige and Skoog (MS) medium for 2 weeks showed a dwarf phenotype with uniformly pale green leaves, indicating that they were less pigmented than wild-type plants (Fig. 2A). When grown in soil for 6 weeks, vegetative rosette leaves of the *chl27-t* plants were curved, with a uniformly pale green color (Fig. 2B). During reproductive development, *chl27-t* plants began flowering much later than wild-type plants, and at this time they had curved cauline leaves of a pale green color, short inflorescence stems and crooked siliques (Fig. 2C, D). In contrast, heterozygous *chl27-t* plants exhibited the same phenotypes as wild-type plants (data not shown). Progeny of heterozygous *chl27-t* plants exhibited a 3:1 ratio of wild-type to *chl27-t* phenotypes, suggesting that the *chl27-t* mutation is inherited in a single recessive manner and that it is linked to the *chl27-t* phenotype (data not shown). This result supports the hypothesis that the T-DNA insertion in the promoter region of *CHL27* results in a reduction of *CHL27* mRNA and leads to the growth retardation of homozygous *chl27-t* plants.

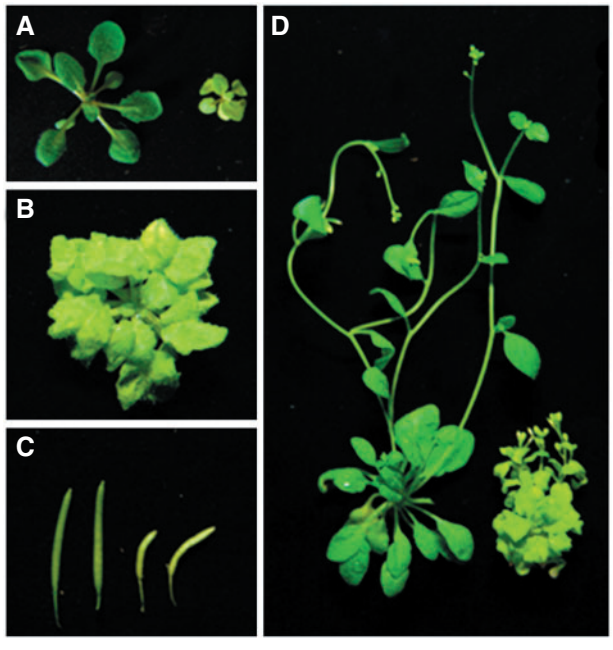

Fig. 2 Phenotypes of the *chl27-t* mutant. (A) Wild-type (left) and *chl27-t* (right) plants grown in MS medium for 2 weeks. The *chl27-t* plant shows a dwarf phenotype with a pale green appearance. (B) A *chl27-t* plant grown in soil for 6 weeks has circinate leaves and shows a delayed flowering time compared with wild-type plants. (C) The phenotype of wild-type (left) and *chl27-t* (right) siliques. *chl27-t* siliques are crooked. (D) Comparison of wild-type (left) and *chl27-t* mutant (right) inflorescence stems. The stems of *chl27-t* plants are shorter than wild-type stems.

Complementation of the chl27-t mutant

To confirm that the T-DNA insertion in *CHL27* is responsible for *chl27-t* phenotypes, we performed a complementation analysis of the *chl27-t* mutant with three constructs: *35S-GFP*, *35S-CHL27-GFP* and *native-CHL27-GFP* (Fig. 3A). The green fluorescent protein (GFP) reporter was fused to the C-terminus of CHL27 to generate the chimeric protein CHL27–GFP to avoid blocking the N-terminal region of CHL27, which contains a chloroplast transit peptide consisting of 39 amino acids (Fig. 4). As shown in Fig. 3B, the expression of *CHL27-GFP* driven by the native *CHL27* promoter or by the constitutive *35S* promoter suppressed the *chl27-t* mutant phenotypes, whereas the expression of *GFP* under the *35S* promoter did not. The wild-type phenotype of the *chl27-t*/*native-CHL27-GFP* transformant indicates that disruption of the *CHL27* promoter by the T-DNA insertion has a critical effect on *CHL27* expression and results in the *chl27-t* mutant phenotype. Expression of the constructs in transformants was assessed by protein gel blot analysis using a monoclonal anti-GFP antibody (Fig. 3C). As expected, the anti-GFP antibody detected the CHL27–GFP protein in all transformants including *35S-CHL27-GFP* or *native-CHL27-GFP* plants, while GFP alone was detected only in *35S-GFP* transformants. Altogether, these results demonstrate that the *chl27-t* mutant is a knock-down mutant of the aerobic MPE cyclase encoded by the *CHL27* gene.

The N-terminal 39 amino acids are essential for the chloroplast localization of CHL27

CHL27 is known to be targeted to the chloroplast and has been suggested to contain an N-terminal chloroplast transit peptide (Moseley et al. 2002, Tottey et al. 2003). To determine the transit peptide of CHL27, the subcellular localization of each of the CHL27 truncation mutants was analyzed by transient expression of GFP fusion proteins in *Arabidopsis* protoplasts. Chl autofluorescence (CHL) and red fluorescence from RFP (red fluorescent protein) were used as controls for chloroplast and cytoplasm, respectively. As shown in Fig. 4A, CHL27 was targeted to the chloroplast when GFP was fused to the C-terminus of CHL27, whereas CHL27 was distributed uniformly in the cytosol when GFP was fused to its N-terminus, indicating that the N-terminus of CHL27 contains a putative

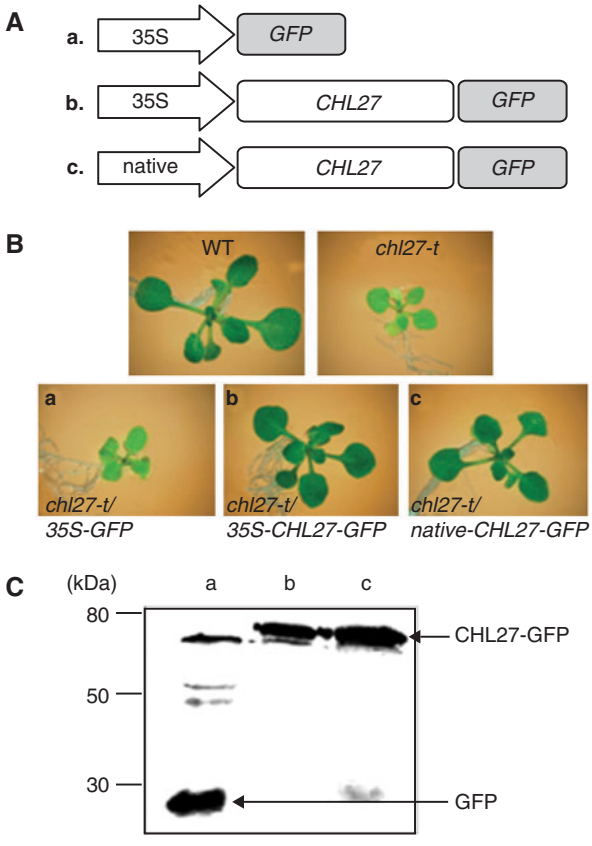

Fig. 3 Complementation analysis of the *chl27-t* mutant with the *CHL27* gene. (A) Schematic diagrams show three constructs for the complementation experiment. *CHL27-GFP* is controlled by the native *CHL27* promoter (c) or the constitutive *35S* promoter (b) in the *native-CHL27-GFP* and *CaMV 35S-CHL27-GFP* constructs, respectively. *GFP* controlled by the *35S* promoter was used as a control (a). (B) Phenotypes of the three transformants (a, b and c). Transformant a exhibited the *chl27-t* mutant phenotype, whereas the other two transformants b and c had wild-type phenotypes, indicating complementation of the *chl27-t* mutation with the *CHL27* gene. (C) Protein gel blot analysis of the three transformants. Total proteins were loaded on a 12% SDS–polyacrylamide gel and transferred onto a nitrocellulose membrane. An anti-GFP monoclonal antibody was used for detection of both CHL27–GFP and GFP proteins, and protein bands were visualized with a ChemiDoc XRS image analysis system.

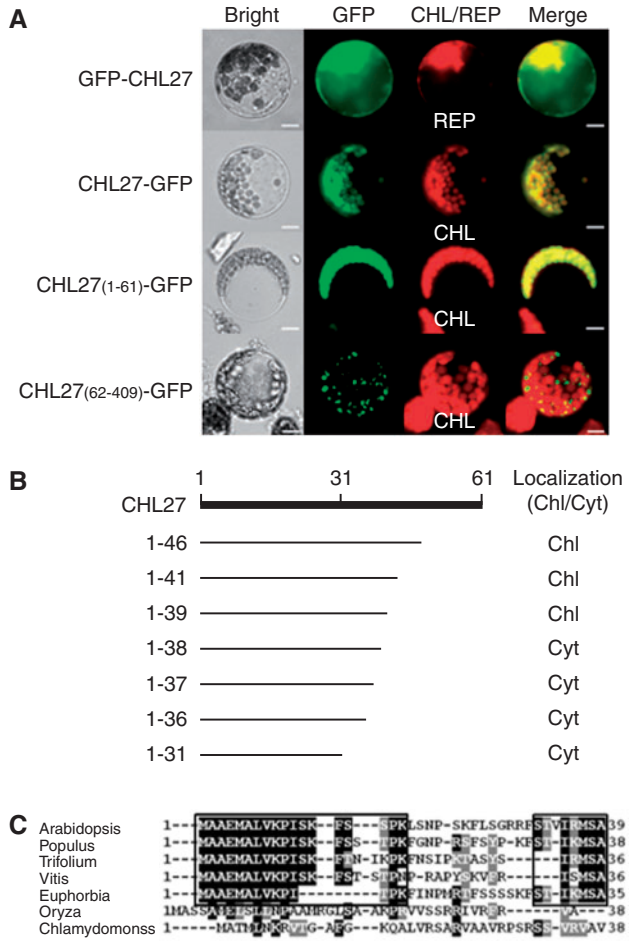

Fig. 4 Identification of the signal peptide for the chloroplast targeting of CHL27. (A) GFP–CHL27 and CHL27–GFP constructs were transiently expressed in *Arabidopsis* protoplasts. The N-terminal region of CHL27 containing a chloroplast transit peptide, $CHL27_{(1–61)}$, was targeted into the chloroplast, but the residual portion of $CHL27_{(62–409)}$ failed to enter the chloroplast and aggregated in the cytoplasm. RFP was used as a control for confirming the cytoplasmic localization of GFP–CHL27, and CHL indicates chloroplasts as detected by Chl autofluorescence. Scale bar = 10 μm. (B) Summary of the subcellular localization of GFP fusion proteins containing various CHL27 N-terminal fragments. Chl and Cyt on the right side of each fragment indicate the chloroplast and cytoplasm, respectively. (C) Alignment of amino acid sequences of the chloroplast-targeting peptide of *Arabidopsis* CHL27 with those of other plants and algae. The N-terminal 39 amino acid residues of *Arabidopsis* CHL27, essential for chloroplast localization, were aligned with other CHL27 orthologs from *Populus trichocarpa, Trifolium repens, Vitis vinifera, Euphorbia esula, Oryza sativa* and *Chlamydomonas reinhardtii*. Conserved sequences in the region are boxed.

chloroplast transit peptide. When two GFP fusion constructs generating chimeric proteins, such as $CHL27_{(1–61)}$–GFP and $CHL27_{(62–409)}$–GFP, were used for the protoplast transformation, $CHL27_{(1–61)}$–GFP was specifically targeted to chloroplasts, whereas the $CHL27_{(62–409)}$–GFP showed a punctate staining pattern, implying that it aggregated in the cytosol (Fig. 4A). To define further the chloroplast transit peptide portion of CHL27, seven deleted mutants from the $CHL27_{(1–61)}$ fragment were obtained by fusing a serial deletion of CHL27 N-terminal fragments to GFP, and introduced into the protoplasts. From this it was demonstrated that the N-terminal 39 amino acids at least were necessary as a chloroplast transit peptide in order to target CHL27 to the chloroplast (Fig. 4B). The N-terminal region of *Arabidopsis* CHL27 is well conserved among various CHL27 homologs, except for rice and *Chlamydomonas* (Fig. 4C).

The chl27-t mutant shows a high Chl a/b ratio and defects in the PSII reaction center

The CHL27 protein has been reported to be essential for Chl biosynthesis by catalyzing the conversion of MPE to protochlorophyllide *a* (Tottey et al. 2003, Rzeznicka et al. 2005). As homozygous *chl27-t* plants were clearly less pigmented than the wild-type plants (Fig. 2), we examined Chl contents in both *chl27-t* mutant and wild-type plants (Table 1). At the same age, the total Chl content per unit fresh weight of leaves in *chl27-t* plants was remarkably decreased (<30%) as compared with that of wild-type plants, and the Chl *a* and *b* levels were also decreased. The Chl *a*/*b* ratio, however, was higher in *chl27-t* plants than in wild-type plants, indicating that the *chl27-t* mutation affects the production of Chl *b* from Chl *a*. In addition to the Chl-depleted phenotype, we observed anomalous accumulation of MgP/MPE after feeding with 5-aminolevulinate (Supplementay Fig. S2).

The depletion of Chl may also affect the photosynthetic efficiency of PSII reaction centers in the *chl27-t* mutant. To assess the photosynthetic performance of the *chl27-t* mutant, Chl fluorescence was analyzed by using a pulse amplitude modulation (PAM) Chl fluorometer (Goh et al. 1999), and a comparison of Chl fluorescence parameters in wild-type and *chl27-t* plants is summarized in Fig. 5. The leaves from wild-type and *chl27-t* plants were dark-adapted for 10 min prior to fluorescence recording, and then a saturating light pulse was applied to determine maximum fluorescence (F_m) and variable fluorescence (F_v) ($F_v = F_m - F_o$). The maximum quantum yield (F_v/F_m) of the PSII of *chl27-t* plants was about 0.33, a considerably lower value than 0.83 found in the wild-type plants, which is the normal value shown in mesophyll cells of most plant species (Fig. 5A). During illumination with actinic light, their maximal fluorescence yields (F_m') were assessed in a time-dependent manner. This showed that the PSII quantum yield ratio [$\Delta F/F_m' = (F_m' - F)/F_m'$] was also remarkably low in *chl27-t* mutant plants as compared with wild-type plants (Fig. 5A). Both ETR (relative electron transport rate) (Fig. 5B) and NPQ (non-photochemical quenching) (Fig. 5C) data also showed considerable differences between wild-type and *chl27-t* plants. These results indicate that the *chl27-t* mutant exhibits low photosynthetic activity caused by damage in the PSII reaction centers.

Table 1 The content of total Chl, Chl *a* and Chl *b*, and Chl *a*/*b*

Line	Chl (mg mg^{-1} FW)			Chl *a*/*b*
	Total Chl	Chl *a*	Chl *b*	
Wild type	1.41 ± 0.11	1.05 ± 0.08	0.36 ± 0.03	2.91 ± 0.10
chl27-t	0.40 ± 0.07	0.34 ± 0.06	0.06 ± 0.01	5.36 ± 0.22

Data are means ± SD ($n = 8$).

chl27-t thylakoids are stroma exposed and lack starch granules

Chloroplast development relies on the coordinated synthesis of Chls and thylakoid proteins, and on their integration and assembly in chloroplast thylakoids (Allen and Forsberg 2001). As *chl27-t* plants showed defects in the production of both Chls and mRNAs encoding thylakoid proteins (Fig. 7, Tables 1 and 2), we examined the

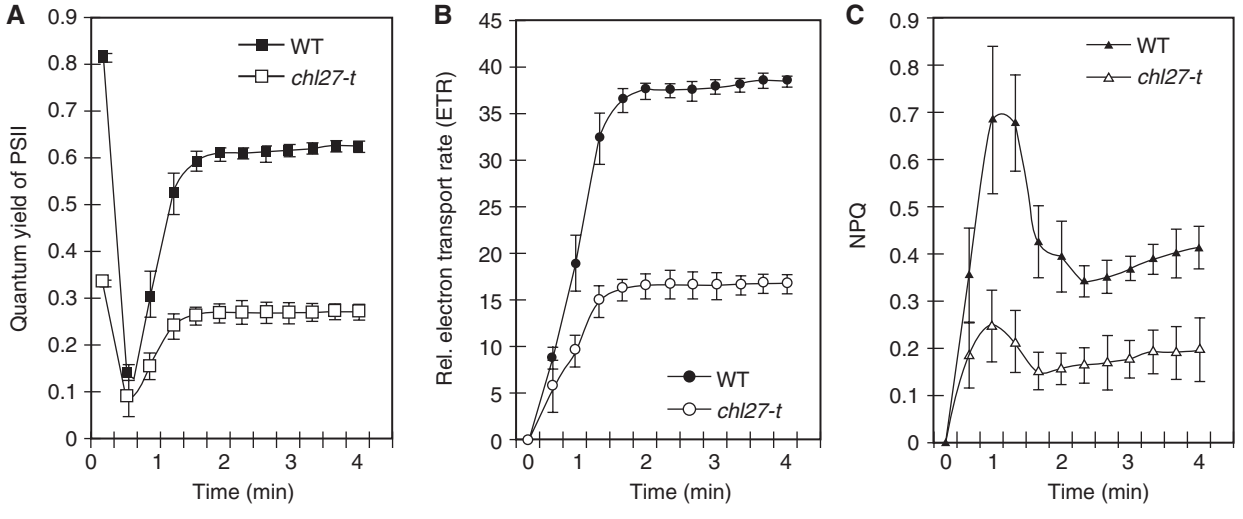

Fig. 5 Fluorescence parameters of wild-type and mutant *chl27-t* plants. (A) Effective PSII quantum yield, $\Delta F/F_m' = (F_m' - F)/F_m'$. (B) Relative electron transport rate, ETR = $\Delta F/F_m' \times$ PAR $\times$ *c* (PAR is the photon flux density of incident light as photosynthetically active radiation, and the constant *c* corresponds to the absorption factor). (C) Non-photochemical quenching, NPQ = $(F_m - F_m')/F_m'$. The displayed data are the means ± SD for wild-type plants ($n = 7$) and the *chl27-t* mutant ($n = 7$).

chloroplast morphology of the *chl27-t* mutant by transmission electron microscopy. Micrographs of leaf sections of *chl27-t* plants showed that their chloroplast morphology was very different from that of wild-type plants (Fig. 6). Wild-type chloroplasts had a normally developed thylakoid membrane system and large starch granules (Fig. 6A). In contrast, the abnormal chloroplasts from *chl27-t* plants were small and irregular in shape, and contained few starch granules (Fig. 6B), a phenotype that may result from low photosynthetic activity (Fig. 5). In addition, the thylakoid membranes were poorly developed and were severely altered in arrangement and distribution. In particular, most *chl27-t* chloroplasts contained only stroma-exposed thylakoids and no normal granal thylakoids due to the unstacking of thylakoid membranes (Fig. 6D), whereas wild-type chloroplasts had normally stacked granal thylakoids (Fig. 6C). Thus, the *chl27-t* mutation causes the Chl deficiency, and eventually leads to defects in chloroplast development.

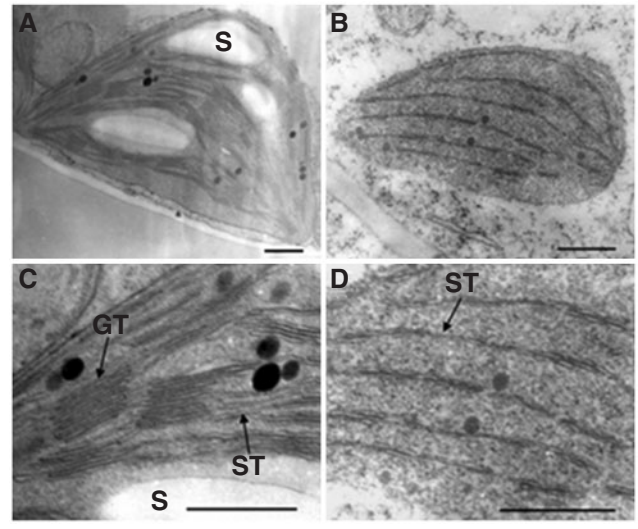

Fig. 6 Transmission electron micrographs of chloroplasts in wild-type (A and C) and *chl27-t* (B and D) plants. C and D are magnifications of A and B, respectively. S, GT and ST indicate starch granules, granal thylakoids and stroma-exposed thylakoids, respectively. Scale bar = 0.5 μm.

Does the chl27-t mutation affect retrograde signaling?

Based on the defective chloroplasts of the *chl27-t* mutant (Fig. 6), we used RNA gel blot analysis to determine whether this mutant could carry out chloroplast to nucleus retrograde signaling. As shown in Fig. 7, the mRNA levels of nuclear genes encoding chloroplast-targeted proteins such as Lhcb1 (a component of the LHCs) (Jansson 1999) and CAO (*Arabidopsis* Chl *a* oxygenase) (Espineda et al. 1999) were remarkably decreased in the *chl27-t* mutant as compared with wild-type plants. However, the expression of both the *ATP2* gene encoding the β-subunit of mitochondrial ATP synthase (Heazlewood et al. 2003) and the *Actin2* gene, used as controls, was not significantly changed in the *chl27-t* mutant compared with wild-type plants (Fig. 7). These results indicate that the defective chloroplasts of the *chl27-t* mutant may send retrograde signals to the nucleus, resulting in a reduced expression of nuclear genes encoding chloroplast-targeted proteins. This proposal is consistent with the decreased mRNA level of *CAO* (Fig. 7), responsible for the conversion of Chl *a* to Chl *b* and for the increased Chl *a*/*b* ratio in *chl27-t* plants (Table 1). In short, the reduced level of *CAO* mRNA may lead to a defect in the conversion of Chl *a* to Chl *b* in *chl27-t* mutants.

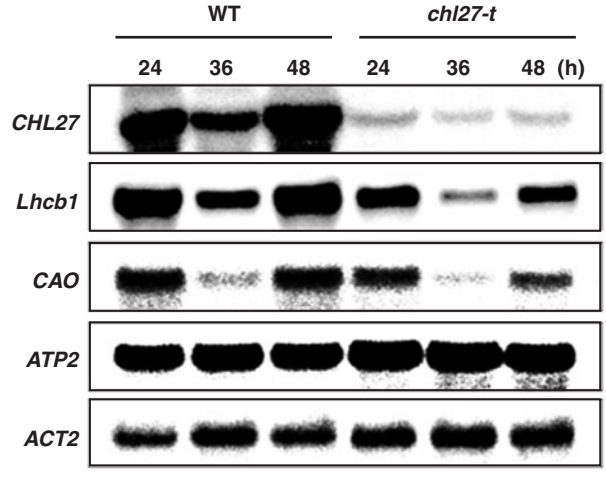

Fig. 7 RNA gel blot analysis of selected transcripts in wild-type and *chl27-t* plants. Wild-type and *chl27-t* seedlings were grown under 12 h light and 12 h darkness for 7 d and then transferred to continuous light. At the time (h) indicated, leaves were harvested and RNAs were isolated. Total RNAs (20 μg) were electrophoresed on an agarose gel, transferred to a membrane and probed with ^{32}P-labeled probes for *CHL27*, *Lhcb1* (At1g29920), *CAO* (At1g44446), *ATP2* (At5g08670) and *ACT2*. *ACT2* was used as a control for equal loading of RNA in each lane.

Transcriptome profiling of the chl27-t mutant suggests defects in PSI and PSII

To determine further the transcriptome profile of nuclear genes whose expression is regulated by retrograde signaling, we performed microarray analysis using the OpArray *Arabidopsis* 29K oligo chip containing 30,384 probes. For reproducibility, we performed triplicated microarray analyses including a dye-swapping experiment and biological replicates. These analyses showed that in the homozygous *chl27-t* mutant, 1,326 genes (*P*-value <0.02, Supplementary Tables S1 and S2) exhibited a >2-fold change in their level of expression (repressed, 689; induced, 637), relative to wild-type plants. Consultation of databases for the functional annotation of *Arabidopsis* genes allowed classification of the induced genes in the *chl27-t* mutant into several categories (Fig. 8A). Among these, stress- and

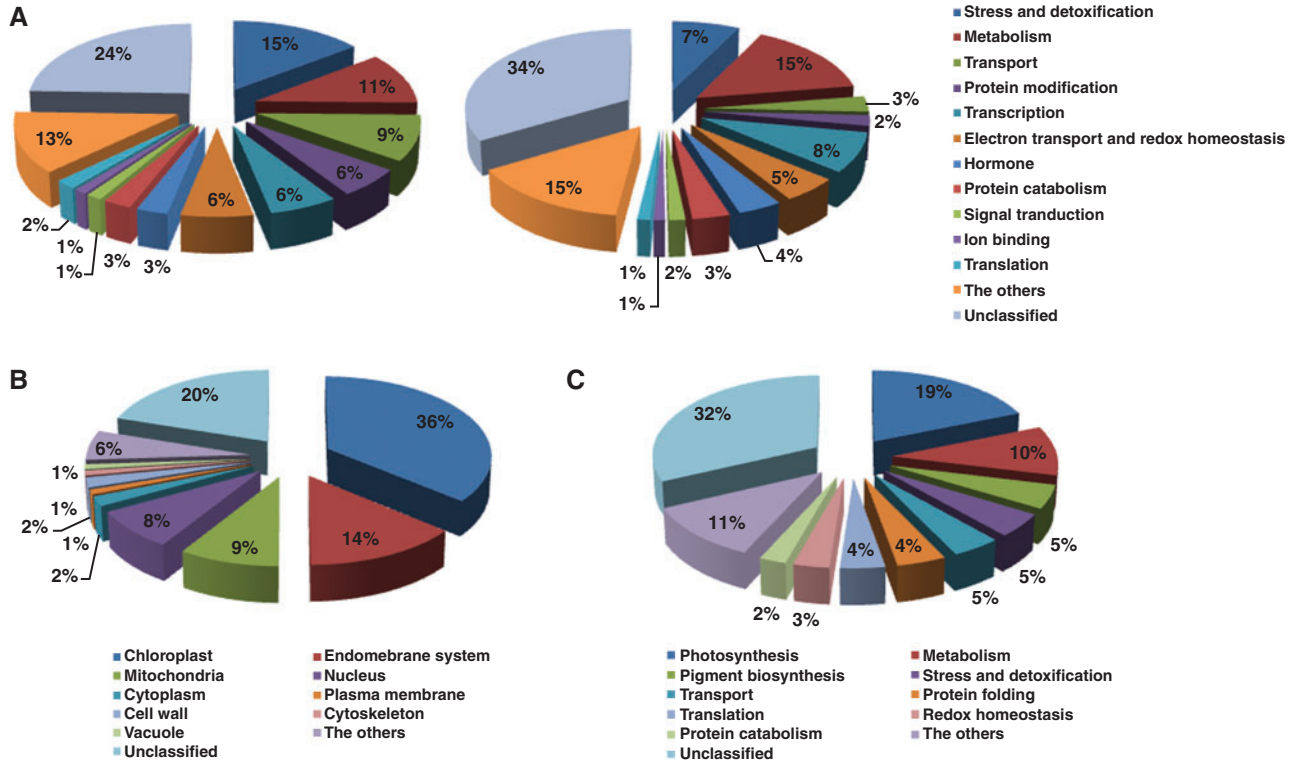

Fig. 8 Classification of genes with altered levels of expression in the *chl27-t* mutant. (A) Functional classification of genes induced (left) or repressed (right) in the *chl27-t* mutant. (B) Ontological classification of genes repressed in the *chl27-t* mutant. (C) Functional classification of genes encoding chloroplast-targeting proteins, sorted by the ontological classification of B.

detoxification-related genes (15%), such as glutathione *S*-transferase and peroxidase, were especially prominent (Fig. 8A and Supplementary Table S1).

According to the ontological categories (Fig. 8B), among the 689 genes repressed in the *chl27-t* mutant, 250 function in the chloroplast (36%), and these were further classified into several functional categories (Fig. 8C) including photosynthesis, pigment (Chl and carotenoid) biosynthesis, stress and detoxification, metabolism, protein folding, transport, redox homeostasis, translation and protein catabolism. Of the 250 chloroplast genes, many photosynthetic genes (19%) were also shown to be repressed in the *chl27-t* mutant, compared with wild-type plants (Fig. 8C), and some representative genes are summarized in Table 2. These include genes encoding subunits of PSI and PSII, electron carriers, components of the LHC, ATP synthase, ferredoxin-NADP$^+$ reductase and enzymes involved in carbon fixation. In particular, six genes (At4g02770, At1g03130, At2g20260, At1g52230, At5g64040 and At2g46820) specify subunits of PSI (PSI-D1, -D2, -E, -H, -N and -P), suggesting that the PSI reaction centers of the *chl27-t* mutant are damaged. Moreover, we found that five other genes (At2g30790, At1g77090, At3g55330, At1g14150, At3g21055) encoding subunits of PSII (PSII-P, -Q, and -T) were also down-regulated in the *chl27-t* mutant, as compared with wild-type plants (Table 2). These findings support the idea that the *chl27-t* mutant is defective in PSII reaction centers, consistent with the results of the Chl fluorescence analysis (Fig. 5).

Repression of genes for pigment biosynthesis, cold acclimation and iron acquisition in the chl27-t mutant

In addition to photosynthetic genes (Table 2), representative genes that belong to other categories are summarized in Table 3, and the expression of a few of these was confirmed by RT–PCR (Fig. 9). As expected from RNA gel blot analyses (Fig. 7), the expression of the *CHL27* and *CAO* genes responsible for Chl biosynthesis was down-regulated 5- and 2.6-fold, respectively. Among Chl biosynthetic genes repressed in the *chl27-t* mutant, the *PORA* gene encoding NADPH-protochlorophyllide oxidoreductase A was more strongly down-regulated (6.2-fold) than was *CHL27* (5-fold).

Besides these, five genes that belong to the stress tolerance and detoxification or to the redox homeostasis functional categories were significantly repressed in the *chl27-t* mutant. Among these, three (At2g42540, At1g29395 and At1g29390) comprised *COR15A* (6-fold), *COR414*

Table 2 Photosynthetic genes repressed in the *chl27-t* mutant

Description	AGI[a]	FC[b]	*P*-value[c]
PSI			
PSI reaction center subunit (PSI-N)	At5g64040	–4.3	0.0163
PSI reaction center subunit II (PSI-D2)	At1g03130	–4.0	0.0144
PSI reaction center subunit (PSI-P)	At2g46820	–3.7	0.0108
PSI reaction center subunit IV (PSI-E)	At2g20260	–2.7	0.0127
PSI reaction center subunit VI (PSI-H2)	At1g52230	–2.4	0.00458
PSI reaction center subunit II (PSI-D1)	At4g02770	–2.0	0.00705
PSII			
PSII oxygen-evolving complex 23 (PSII-P)	At2g30790	–3.6	0.001
PSII oxygen-evolving enhancer 3 (PsbQ)	At1g14150	–3.3	0.0191
PSII oxygen-evolving complex protein (PsbP)	At1g77090	–2.4	0.00389
PSII reaction center, PsbP family protein	At3g55330	–2.4	0.00116
PSII (PSII-T)	At3g21055	–2.3	0.0173
Chl A-B-binding proteins			
Chl *a*/*b*-binding protein (LHCI 2.1)	At1g19150	–4.3	0.00402
Chl *a*/*b*-binding protein (LHCII 4.2)	At3g08940	–3.5	0.0153
Chl *a*/*b*-binding protein CP26, (LHCII 5)	At4g10340	–3.2	0.00815
Chl *a*/*b*-binding protein/LHCI type I (CAB, LHCI 1)	At3g54890	–3.2	0.00273
Chl *a*/*b*-binding protein 165/180, LHCII type I	At1g29920	–3.1	0.00246
Chl *a*/*b*-binding protein/LHCII type I (LHB1B1)	At2g34430	–2.8	0.0101
Electron carriers			
Ferredoxin-related, 2Fe–2S iron–sulfur cluster-binding domains	At3g16250	–3.6	0.00191
Plastoquinone	At5g58260	–3.5	0.00118
Plastocyanin	At1g76100	–2.7	0.00664
ATP synthase and ferredoxin-$NADP^+$ reductase			
γ subunit of chloroplast ATP synthase	At4g04640	–3.3	0.0114
Ferredoxin-NADP(+) reductase	At5g66190	–3.2	0.0102
Carbon fixation			
NADP-dependent glyceraldehydephosphate dehydrogenase	At1g12900	–3.6	0.0114
Sedoheptulose-1,7-bisphosphatase	At3g55800	–3.1	0.00993
Phosphoribulokinase/uridine kinase-related	At1g80380	–3.1	0.00223
Fructose-1,6-bisphosphatase	At3g54050	–2.7	0.00552
Ribose 5-phosphate isomerase	At5g44520	–2.4	0.00233
Ribulose-1,5-bisphosphate carboxylase/oxygenase small subunit	At5g14260	–2.4	0.00537
RuBisCO small subunit 1A	At1g67090	–2.3	0.00373

[a] *Arabidopsis* gene index number.
[b] Fold change is the average of three replicates including a dye-swapping experiment and biological replicates, and generated by comparing the transcript abundance in *chl27-t* plants with that in wild-type plants.
[c] Student's *t*-test *P*-values for data comparison.

(4.2-fold) and *COR314* (2.2-fold) for cold acclimation, and the other two (At5g49730 and At5g49740) consisted of *AtFRO6* (6.2-fold) and *AtFRO7* (3.8-fold), genes that play possible roles in iron acquisition in aerial green tissues.

Discussion

Here, we characterized an *Arabidopsis chl27-t* mutant containing a T-DNA insertion in the *CHL27* promoter. Although previous work reported the antisense mutant (*chl27-as*) lines showing the partial chlorotic phenotype, dependent on the *CHL27* mRNA level (Tottey et al. 2003), our *chl27-t* mutant exhibited various characteristic phenotypes distinct from that of *chl27-as* lines (Fig. 2). Moreover, the T-DNA insertion in a promoter region, very close to the 5′-untranslated region (5′-UTR), led to reduced *CHL27* expression as in *chl27-as* lines, but the *chl27-t* plants still sustained flowering and produced seeds (Fig. 2) despite the reduced photosynthetic efficiency (Fig. 5). Thus, the T-DNA-inserted mutation may be more convenient for the genetic approach for the aerobic cyclase than the antisense method, and, moreover, allowed the complementation

Table 3 Some representative genes repressed in *chl27-t* mutant

Description	AGI[a]	FC[b]	*P*-value[c]
Chl biosynthesis			
NADPH-protochlorophyllide oxidoreductase A (PORA)	At5g54190	–6.2	0.015
Aerobic MPE cyclase (CHL27)	At3g56940	–5.0	0.00756
Magnesium-protoporphyrin *O*-methyltransferase (CHLM)	At4g25080	–2.8	0.000523
Chl *a* oxygenase (CAO)	At1g44446	–2.6	0.00703
3,8-Divinyl protochlorophyllide *a* 8-vinyl reductase (PCB2)	At5g18660	–2.5	0.000827
Mg-protoporphyrin IX chelatase (CHLH, GUN5)	At5g13630	–2.3	0.00496
Uroporphyrinogen decarboxylase	At3g14930	–2.2	0.0186
Carotenoid biosynthesis			
9-*cis*-Epoxycarotenoid dioxygenase (NCED4)	At4g19170	–4.7	0.00103
Violaxanthin de-epoxidase precursor (NPQ1)	At1g08550	–3.2	0.0134
Lycopene epsilon cyclase (LUT2)	At5g57030	–2.4	0.00103
Phytoene synthase (PSY)	At5g17230	–2.3	0.016
Zeaxanthin epoxidase (ABA1)	At5g67030	–2.1	0.000404
Cold acclimation			
Cold-responsive protein (COR15A)	At2g42540	–6.0	0.00762
WCOR413-like protein gamma form (COR414-TM1)	At1g29395	–4.2	0.00228
WCOR413-like protein gamma form (COR314-TM2)	At1g29390	–2.2	0.00245
Iron acquisition			
Ferric chelate reductase 6 (AtFRO6)	At5g49730	–6.2	0.0058
Ferric chelate reductase 7 (AtFRO7)	At5g49740	–3.8	0.00489

[a] *Arabidopsis* gene index number.
[b] Fold change is the average of three replicates including a dye-swapping experiment and biological replicates, and generated by comparing the transcript abundance in *chl27-t* plants with that in wild-type plants.
[c] Student's *t*-test *P*-values for data comparison.

analysis to be performed, confirming that this mutation leads to a knock-down effect of the *CHL27* gene that resulted in retarded growth and Chl depletion (Figs. 2 and 3, and Table 1).

The growth retardation of the *chl27-t* mutant may be primarily due to the defects of Chl biosynthesis. Previously, 5-aminolevulinate-fed *chl27-as* lines were found to accumulate MPE, a substrate for the cyclase reaction, and homologs of *CHL27* have been reported to encode a membrane subunit of aerobic MPE cyclase, which is involved in Chl production (Tottey et al. 2003, Rzeznicka et al. 2005). We also confirmed accumulation of excess porphyrin precursors including MPE in *chl27-t* plants through a preliminary feeding experiment with 5-aminolevulinate (Supplementary Fig. S2). Thus, these observations suggest that the *chl27-t* mutation may affect the catalytic activity of cyclase, resulting in a blockage of the Chl biosynthetic pathway. This conclusion is clearly supported by the Chl fluorescence analysis, which showed a reduced photosynthetic efficiency of PSII in the *chl27-t* mutant (Fig. 5). This result is highly consistent with microarray data that showed the reduced expression of genes encoding subunits of PSII and LHCII in the *chl27-t* mutant (Table 2). The *chl27-as* mutant was also reported to have a severely damaged PSI reaction center, with a depletion of the core proteins of LHCI and PSI (Tottey et al. 2003). Although we did not directly examine the PSI activity of the *chl27-t* mutant in this study, the reduced levels of *LHCI* and *PSI* mRNAs in our microarray data (Table 2) confirm the hypothesis that the *chl27-t* mutant may also have a severely damaged PSI reaction center, like the *chl27-as* mutant. Taken together, we assume that the blockage of Chl biosynthesis caused by the *chl27-t* mutation may reduce the photosynthetic activities of both PSI and PSII, thus retarding the growth of *chl27-t* plants.

Transmission electron micrography demonstrated that the pale green leaves of *chl27-t* plants exhibited abnormal chloroplast morphologies (Fig. 6B). In particular, most *chl27-t* chloroplasts lacked normal granal thylakoids but contained only stroma-exposed thylakoids and unstacked thylakoid membranes (Fig. 6D). The stacking of thylakoid membranes has been suggested to depend on thylakoid proteins including LHCII, which is stabilized by Chl *b* (Allen and Forsberg 2001, Bumba et al. 2004, Tanaka and Tanaka 2007). The unstacking of thylakoid membranes in the chloroplasts of *chl27-t* plants may be due to defects in the synthesis of Chl *b* and of cognate proteins including those in LHCII. Thus, these observations are consistent

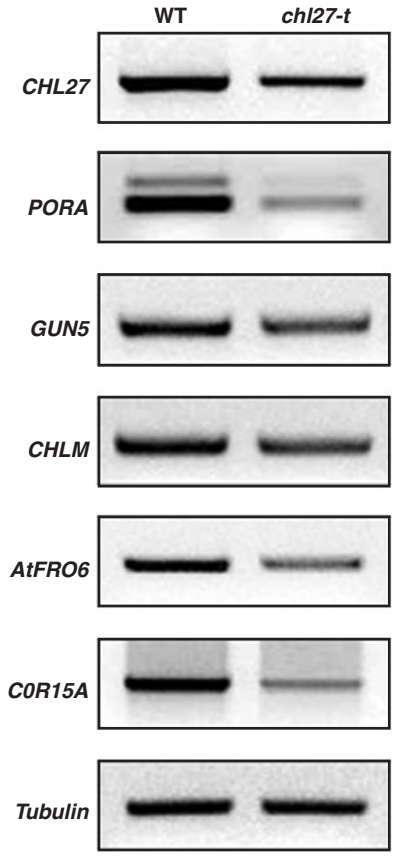

Fig. 9 RT–PCR analysis of selected genes identified by microarray analysis. Transcript levels for several genes listed in Table 3 were determined by RT–PCR, using 5 μg of total RNA for each reverse transcription reaction. The *tubulin* level was used as an internal control to normalize the amount of cDNA template.

with the idea that the *chl27-t* mutation causes a depletion of Chl *b* (Table 1) and a reduction of *LHCII* mRNAs (Fig. 7 and Table 2).

The vast majority of chloroplast proteins are encoded by the nuclear genome. These proteins are targeted into chloroplasts as a precursor protein with a cleavable N-terminal transit peptide, essential for chloroplast localization (Bruce 2000). CHL27, a chloroplast protein, is predicted to contain an N-terminal transit peptide, consisting of 36 amino acids, determined by using TargetP 1.1, a subcellular localization program (Emanuelsson et al. 2007). However, in contrast to this prediction, the N-terminal segment with 36 amino acids in *Arabidopsis* CHL27 failed to enter the chloroplast (Fig. 4B). For correct targeting of CHL27 to the chloroplast, at least 39 amino acids were necessary for a chloroplast transit peptide (Fig. 4B). Moreover, the N-terminal region of *Arabidopsis* CHL27 was highly conserved among CHL27 homologs of dicotyledonous plants, except for the rice CHL27 and Crd1, a CHL27 homolog of green algae (Fig. 4C). Interestingly, despite high similarity (>80%) among the CHL27 homologs from *Arabidopsis*, rice and green algae, no significant homology was found in their putative transit peptide portion. This suggests that the transit peptides had been greatly influenced evolutionarily during the endosymbiosis of the photosynthetic eukaryote with the prokaryote, an origin of the chloroplast, and thus the species-specific transit peptide may reflect distant properties in the chloroplast-targeting mechanism.

In addition, chloroplasts send signals to the nucleus to control the expression of nuclear genes encoding chloroplast-targeting proteins by a process called retrograde signaling (Nott et al. 2006). We also discovered that nuclear genes encoding chloroplast-targeting proteins such as LHCB1 and CAO were repressed (Fig. 7), suggesting that the *chl27-t* mutant affects retrograde signaling. Furthermore, our microarray analysis showed significant changes in expression of numerous genes in the *chl27-t* mutant, compared with the wild type (Fig. 8, and Tables 2 and 3). Of the induced genes, many could be categorized as stress- and detoxification-related genes (15%), such as glutathione *S*-transferase and peroxidase (Fig. 8A and Supplementary Table S1). Presumably, the *chl27-t* mutant is partially under photo-oxidative stress as secondary effects, and thus these genes may be induced for cell defense and survival under photo-oxidative stress, similar to the activation of genes encoding heat shock proteins in response to mitochondrial impairment in maize that leads to production of reactive oxygen species (Kuzmin et al. 2004).

In the case of the down-regulated genes, we focused on those involved in two intracellular activities, Chl biosynthesis and iron acquisition. First, most of the genes for Chl biosynthesis, as shown in Figs. 7 and 9, and Table 3, fell into the c1 cluster, composed of four genes: *HEMA1*, *GUN5* (*CHLH*), *CHL27* and *CAO*. The genes are known to be rapidly induced by light and to fluctuate synchronously under diurnal and circadian rhythm, and encode the key enzymes in the Chl biosynthetic pathway (Matsumoto et al. 2004). The *chl27-t* mutation is likely to affect mainly the expression level of c1 cluster genes, the most important regulatory genes in Chl biosynthesis. However, the *PORA* gene (6.2-fold), which belongs to the c4 cluster, was more significantly repressed than were c1 cluster genes (Fig. 9 and Table 3). A few studies have reported that specific enzyme pairs involved in tetrapyrrole synthesis form protein complexes for stimulating enzyme activity (Tanaka and Tanaka 2007). For example, it has been reported that the CHLH subunit of magnesium chelatase interacts with a magnesium-protoporphyrin *O*-methyltransferase (CHLM), which uses the product of the CHLH as its substrate, and that the CHLH enhances the activity of the CHLM enzyme, suggesting complex formation between CHLH and CHLM (Hinchigeri et al. 1997, Shepherd et al. 2005). There have

also been similar cases such as GluTR and GSA-AT, and PPOX and FeCh in tetrapyrrole synthesis (Hinchigeri et al. 1997, Moser et al. 2001, Koch et al. 2004, Lüer et al. 2005, Nogaj and Beale 2005, Shepherd et al. 2005, Tanaka and Tanaka 2007). Recently, Nagata et al. (2007) revised the conventional order of enzymatic steps in the Chl biosynthetic pathway by the substrate specificity of 8-vinyl reductase (DVR) to place the cyclase reaction just before the POR reaction, i.e. 3,8-divinyl protochlorophyllide *a*, the product of aerobic MPE cyclase (CHL27), is used as a substrate for POR. In this respect, the strong repression of the *PORA* gene caused by the *chl27-t* mutation leads us to speculate that complex formation between CHL27 and POR may improve the efficiency of Chl biosynthesis.

Secondly, we observed that the *chl27-t* mutation led to the remarkable repression of the *AtFRO6* and *AtFRO7* genes (Fig. 9 and Table 3) that play a possible role in iron acquisition for cellular activities including respiration, photosynthesis and Chl biosynthesis (Feng et al. 2006), and it seems that the *chl27-t* mutant has an imbalance in iron homeostasis. PSI has been reported to be the major sink for iron in all oxygenic photoautotrophs (Jordan et al. 2001) and, thus, the repression of genes for the PSI subunits (Table 2) may affect the iron homeostasis in the *chl27-t* mutant, resulting in the repression of genes involved in iron acquisition. Interestingly, the *AtFRO6* (6.2-fold) gene was more significantly repressed than *AtFRO7* (3.8-fold) in the *chl27-t* mutant (Table 3). *AtFRO6* and *AtFRO7* have been reported to encode highly identical (>90%) ferric chelate reductases and to show the same expression patterns, which are dependent on light, and are suggested to localize to the chloroplast or to plasma membrane (Feng et al. 2006, Mukherjee et al. 2006). However, despite the high similarity in protein sequence and gene expression patterns between AtFRO6 and AtFRO7, they have different FRO activities: AtFRO6 showed the lowest FRO activity among eight AtFROs identified, whereas AtFRO7 displayed considerable FRO activity (Wu et al. 2005, Feng et al. 2006). This suggests that AtFRO6 may have another specific role in green aerial tissues besides the basic role in iron acquisition, whereas AtFRO7 may play a main role in the iron acquisition for the diverse cellular activities in green aerial tissues. Based on the higher repression of *AtFRO6* (6.2-fold) than of *AtFRO7* (3.8-fold) in the *chl27-t* mutant, AtFRO6 may be tightly associated with the aerobic MPE cyclase reaction, which has been reported to depend on iron and oxygen (Nasrulhaq-Boyce et al. 1987). Furthermore, the CHL27 protein, a membrane subunit of aerobic cyclase, contains consensus D/EExxH motifs specific to carboxylate-liganded di-iron-binding enzymes, and thus it has been suggested to require iron during the cyclase reaction (Moseley et al. 2000, Tottey et al. 2003). Taken together, we propose that AtFRO6 may have a role in assisting the cyclase reaction mediated by CHL27.

Aerobic MPE cyclase was recently reported to exist in chloroplasts as a membrane-interacting multisubunit enzyme containing at least one soluble and two membrane-bound components (Rzeznicka et al. 2005). Moreover, it has been suggested that the aerobic cyclase complex, in addition to CHL27, might be composed of a substrate-binding protein, regulatory subunits or reductase, but these other components remain to be characterized. In view of this, our complementation analysis demonstrating functional activity of the fused protein, CHL27–GFP as shown in Fig. 3, is very important since this will allow us potentially to isolate the other components of aerobic MPE cyclase by both pull-down experiments with anti-GFP and the tandem affinity purification method, and to identify them thereafter via mass spectrometry.

Materials and Methods

Plant materials and growth conditions

The *chl27-t* mutant, an *Arabidopsis* T-DNA insertion line, was identified by searching the insertion flanking sequence database (http://www.arabidopsis.org/) using the *CHL27* cDNA as query sequence, and seeds were obtained from the Salk Institute Genomic Analysis Laboratory collection (Alonso et al. 2003). Homozygous T_3 *chl27-t* plants were selected by PCR genotyping analysis, and T_4 *chl27-t* plants were generated by self-pollination of homozygous T_3 plants. For microarray, RT–PCR and RNA gel blot analyses, seeds from homozygous *chl27-t* plants were sown in soil or onto medium (pH 5.6) containing MS salts and grown in a controlled growth chamber (22°C, 70% humidity and illumination of 70–80 μmol m^{-2} s^{-1} white light) with 16 h light and 8 h darkness. For photoperiodic treatments, seeds from individual plants were sown onto MS medium and grown in a growth chamber with 12 h light and 12 h darkness for 7 d, followed by growth under continuous light.

Transient expression of GFP fusion proteins

CHL27 inserts for the various GFP fusion constructs were prepared by PCR, and the PCR products were cloned into the vector pENSOTG provided by Hisashi Koiwa (Texas A&M University, USA) (Koiwa et al. 2004). The resulting constructs (20 μg) were introduced into *Arabidopsis* protoplasts by polyethylene glycol-mediated transformation as described (Lee et al. 2001). Transformed protoplasts were incubated at 22°C in the dark. Expression of the fusion protein was observed with an Olympus AX-70 fluorescence microscope 2 and 3 d after transformation, and the images were captured with a cooled charge-coupled device camera (Olympus DP-70). The filter sets used were XF116-2 (exciter, 475AF20; dichroic, 500DRLP; emitter, 510AF23), XF33 (exciter, 535DF35; dichroic, 570DRLP; emitter, 605DF50) and XF137 (exciter, 540AF30; dichroic, 570DRLP; emitter, 585ALP) (Omega, Inc., Brattleboro, VT, USA) for GFP, RFP and Chl autofluorescence, respectively. The data were processed using Adobe Photoshop software (Mountain View, CA, USA).

Complementation analysis

A complementation construct for expressing CHL27–GFP was produced by joining PCR fragments of the *CHL27* promoter region (native promoter) and the cDNA encoding CHL27–GFP. The *native-CHL27-GFP*, *35S-GFP* and *35S-CHL27-GFP* cassettes were cloned into the binary vector pBIB-HYG (Becker 1990). The resulting plasmids were introduced into *Agrobacterium* GV3101 and transformed into homozygous *chl27-t* plants via the floral dipping method (Clough and Bent 1998). T_2 seeds from independent T_1 transgenic lines were plated on medium supplemented with 25 μg ml^{-1} hygromycin. The selected T_2 plants were used for protein gel blot analysis, and the phenotypes of T_2 plants were compared with those of wild-type and *chl27-t* plants.

Measurement of Chl content and Chl fluorescence

Chls were extracted from individual leaves with 80% acetone. Chl concentrations per unit of fresh weight of leaves were calculated as described by Arnon (1949). Chl fluorescence parameters were measured with a PAM Chl fluorometer (Heinz Walz GmbH, Effeltrich, Germany) according to Goh et al. (1999). The leaves were dark adapted for 10 min prior to fluorescence recording, and then saturating light pulses (5,000 μmol m^{-2} s^{-1}) inducing maximal fluorescence yields, F_m and F_m', were applied 40 s following the onset of the measuring light (0.8 μmol m^{-2} s^{-1}) and every 20 s after the onset of the actinic light (61.3 μmol m^{-2} s^{-1}). The pre-amplified signal was processed by the PAM control unit, and typical dark–light induction curves were recorded and analyzed with WinControl software (Heinz Walz GmbH, Effeltrich, Germany). For the photosynthetic activity of PSII, the above obtained data were converted into a few fluorescence-derived parameters, which signify the quantum yield, $\Delta F/F_m' = (F_m' - F)/F_m'$, the $\mathrm{ETR} = \Delta F/F_m' \times \mathrm{PAR} \times c$, and $\mathrm{NPQ} = (F_m - F_m')/F_m'$. PAR indicates the photon flux density of incident light as photosynthetically active radiation, and c as constant corresponds to the absorption factor.

Isolation of total RNA, RT–PCR and RNA gel blot analysis

Total RNAs were isolated from wild-type and mutant leaves using TRI-Reagent (Molecular Research Center, Cincinnati, OH, USA) according to the manufacturer's instructions, and 5 μg of total RNA was used for RT–PCR analysis. cDNA was constructed by using AMV reverse transcriptase XL (TAKARA SHUZO CO. LTD., Otsu, Shiga, Japan) and an oligo(dT_{18}) primer, and amplification was performed with the cDNAs and specific primer pairs listed in Supplementary Table S3. Amplification was performed for 25 cycles (95°C for 20 s, 55°C for 40 s and 72°C for 30 s), except for PCR with the *COR15A* primer pair (30 cycles). For reproducibility, the RT–PCR analysis was carried out at least three times, with similar results.

For RNA gel blot analysis, 20 μg of total RNA was fractionated by electrophoresis through a 1.2% formaldehyde–agarose gel and transferred onto a nylon membrane (Schleicher & Schuell BioScience, Inc., Keene, NH, USA) according to a standard method (Sambrook and Russell 2001), and radiolabeled probes were prepared using a random labeling kit according to the manufacturer's instructions (Promega, San Luis Obispo, CA, USA). After hybridization, the membranes were washed with 2× SSC (1× SSC is 0.15 M NaCl and 0.015 M sodium citrate) and 0.1% SDS at room temperature for 20 min and with 0.1× SSC and 0.1% SDS at 60°C for 30 min. Finally, the membrane was exposed to an X-ray film. Bands were quantified with a GS-700 imaging densitometer (BioRad, Hercules, CA, USA).

Protein gel blot analysis

Total protein samples obtained from leaves of individual plants were loaded onto a 12% SDS–polyacrylamide gel and transferred onto a Hybond™-ECL™ nitrocellulose membrane (Amersham Biosciences, Piscataway, NJ, USA) as previously described (Sambrook and Russell 2001). For detection, the nitrocellulose membrane was blocked for 1 h with a blocking buffer containing 5% Difco™ skim milk (BD, Franklin Lakes, NJ, USA) in 1× TBST buffer (10 mM Tris–HCl, pH 8.0, 150 mM NaCl, 0.1% Tween-20), incubated for 1 h in anti-GFP monoclonal antibody (Clontech Inc., Mountain View, CA, USA) diluted 1 : 500 in the blocking buffer and afterwards washed in 1× TBST buffer. Anti-mouse IgG–horseradish peroxidase (HRP) diluted 1: 5,000 in the blocking buffer was used as a secondary antibody. After washing, protein bands were detected using the chemiluminescent substrate ECL™ Western blotting analysis system (Amersham Biosciences) and were visualized using a ChemiDoc XRS image analysis system (BioRad).

Transmission electron microscopy

Leaves from wild-type and *chl27-t* plants were processed for transmission electron microscopy as previously described (Bozzola and Russell 1999). Leaves from 12-d-old plants were fixed in a solution containing 2.5% glutaraldehyde in 0.1 M cacodylate buffer at 4°C for 15 h. They were then washed in 0.1 M cacodylate buffer and further fixed in 1% OsO_4 at 4°C for 15 h. After washing, the samples were dehydrated and embedded in epon resin. Ultra-thin sections were prepared with an ultra-microtome and collected on nickel grids. The sections were stained with uranyl acetate and lead citrate, and examined with a TECNAI transmission electron microscope (120 kV) (Philips, Eindhoven, The Netherlands).

Preparation of fluorescent DNA probes and hybridization

Total RNAs were extracted from wild-type and *chl27-t* leaves using TRI-Reagent (Molecular Research Center) according to the manufacturer's instructions. Fluorescence labeled cDNA probes were prepared from 20 μg of total RNA by oligo(dT_{18})-primed polymerization using SuperScript II reverse transcriptase (Invitrogen, New York, NY, USA) in a total reaction volume of 30 μl. The reverse transcription mixture included 400 U of Superscript RNase H-reverse transcriptase (Invitrogen), 15 mM dATP, dTTP and dGTP, 0.6 mM dCTP and 3 mM Cy3- or Cy5-labeled dCTP (NEN Life Science Product, Inc., Boston, MA, USA). After reverse transcription, the sample RNA was degraded by adding 5 μl of stop solution (0.5 M NaOH/50 mM EDTA) and incubating at 65°C for 10 min. The labeled cDNA mixture was then concentrated using the ethanol precipitation method. The concentrated Cy3- and Cy5-labeled cDNAs were resuspended in 10 μl of hybridization solution (GenoCheck, Ansan, Kyunggi, Korea). The two labeled cDNAs were mixed, and the mixture was denatured at 95°C for 2 min and then incubated in a 45°C water chamber for 20 min. The cDNA mixture was then placed on an OpArray *Arabidopsis* 29K (Operon Biotechnologies, Inc., Huntsville, AL, USA) and covered by a hybridization chamber. The hybridized slides were washed in 2× SSC, 0.1% SDS for 2 min, 1× SSC for 3 min, and then in 0.2× SSC for 2 min at room temperature. The slides were dried by centrifugation at 3,000 r.p.m. for 20 s.

Scanning and data analysis

Hybridized slides were scanned with an Axon Instruments GenePix 4000B scanner, and the scanned images were analyzed with the software programs GenePix Pro 5.1 (Axon, CA, USA)

and GeneSpring GX 7.3.1 (Sillicongenetics, Redwood, CA, USA). No data points were eliminated by visual inspection from the initial GenePix image, and the algorithm was used to eliminate all bad spots. The background signal intensity was determined by including the spotting solution on each slide. To filter out unreliable data, spots with signal-to-noise ratios (signal – background – background SD) <10 were not included. Data were normalized by the global, lowess, print-tip and scaled normalization methods for reliability. Relevant genes were those identified as differing in expression by at least 2-fold in the test and control samples.

Supplementary material

Supplementary material mentioned in the article is available to online subscribers at the journal website www.pcp.oxfordjournals.org.

Funding

The BK21 program (project No. EB-NCRC (#R15-2003-012-01002-0) and EB-NCRC (#R15-2003-012-01002-0) of the Ministry of Education, Science and Technology in Korea.

Acknowledgments

We thank Dr. Hisashi Koiwa at Texas A&M University for the kind gift of vectors pBIB-HYG and pENSOTG, and Dr. Youn Il Park at Chungnam National University and Dr. Chang Hyo Goh at Chonnam National University in Korea for their technical assistance in using the PAM Chl fluorometer.

References

Allen, J.F. and Forsberg, J. (2001) Molecular recognition in thylakoid structure and function. *Trends Plant Sci*. 6: 317–326.

Alonso, J.M., Stepanova, A.N., Leisse, T.J., Kim, C.J., Chen, H., et al. (2003) Genome-wide insertional mutagenesis of *Arabidopsis thaliana*. *Science* 301: 653–657.

Arnon, D.I. (1949) Copper enzymes in isolated chloroplasts. Polyphenoloxidase in *Beta vulgaris*. *Plant Physiol*. 24: 1–15.

Becker, D. (1990) Binary vectors which allow the exchange of plant selectable markers and reporter genes. *Nucleic Acids Res*. 18: 203.

Bozzola, J.J. and Russell, L.D. (1999) Electron Microscopy: Principles and Techniques for Biologists Jones and Bartlett Publishers, Sudbury, MA.

Bruce, B.D. (2000) Chloroplast transit peptides: structure, function and evolution. *Trends Cell Biol*. 10: 440–447.

Buchanan, B.B., Gruissem, W. and Jones, R.L. (2000) Biochemistry & Molecular Biology of Plants American Society of Plant Physiologists, Rockville, MD.

Bumba, L., Husak, M. and Vacha, F. (2004) Interaction of photosystem 2–LHC2 supercomplexes in adjacent layers of stacked chloroplast thylakoid membranes. *Photosynthetica* 42: 193–199.

Chew, A.G. and Bryant, D.A. (2007) Chlorophyll biosynthesis in bacteria: the origins of structural and functional diversity. *Annu. Rev. Microbiol*. 61: 113–129.

Clough, S.J. and Bent, A.F. (1998) Floral dip: a simplified method for Agrobacterium-mediated transformation of *Arabidopsis thaliana*. *Plant J*. 16: 735–743.

Eckhardt, U., Grimm, B. and Hortensteiner, S. (2004) Recent advances in chlorophyll biosynthesis and breakdown in higher plants. *Plant Mol. Biol*. 56: 1–14.

Emanuelsson, O., Brunak, S., von Heijne, G. and Nielsen, H. (2007) Locating proteins in the cell using TargetP, SignalP and related tools. *Nat. Protoc*. 2: 953–971.

Espineda, C., Linford, A., Devine, D. and Brusslan, J. (1999) The *AtCAO* gene, encoding chlorophyll *a* oxygenase, is required for chlorophyll *b* synthesis in *Arabidopsis thaliana*. *Proc. Natl Acad. Sci. USA* 96: 10507–10511.

Feng, H., An, F., Zhang, S., Ji, Z., Ling, H.Q. and Zuo, J. (2006) Light-regulated, tissue-specific, and cell differentiation-specific expression of the *Arabidopsis* Fe(III)-chelate reductase gene AtFRO6. *Plant Physiol*. 140: 1345–1354.

Goh, C.H., Schreiber, U. and Hedrich, R. (1999) New approach of monitoring changes in chlorophyll a fluorescence of single guard cells and protoplasts in response to physiological stimuli. *Plant Cell Environ*. 22: 1057–1070.

Havaux, M. and Tardy, F. (1997) Thermostability and photostability of photosystem II in leaves of the chlorina-f2 barley mutant deficient in light-harvesting chlorophyll a/b protein complexes. *Plant Physiol*. 113: 913–923.

Heazlewood, J.L., Whelan, J. and Millar, A.H. (2003) The products of the mitochondrial orf25 and orfB genes are FO components in the plant F1FO ATP synthase. *FEBS Lett*. 540: 201–205.

Hinchigeri, S.B., Hundle, B. and Richards, W.R. (1997) Demonstration that the BchH protein of *Rhodobacter capsulatus* activates S-adenosyl-L-methionine: magnesium protoporphyrin IX methyltransferase. *FEBS Lett*. 407: 337–342.

Jansson, S. (1999) A guide to the Lhc genes and their relatives in *Arabidopsis*. *Trends Plant Sci*. 4: 236–240.

Jordan, P., Fromme, P., Witt, H.T., Klukas, O., Saenger, W. and Krau, N. (2001) Three-dimensional structure of cyanobacterial photosystem I at 2.5 Å resolution. *Nature* 411: 909–917.

Koch, M., Breithaupt, C., Kiefersauer, R., Freigang, J., Huber, R. and Messerschmidt, A. (2004) Crystal structure of protoporphyrinogen IX oxidase: a key enzyme in haem and chlorophyll biosynthesis. *EMBO J*. 23: 1720–1728.

Koiwa, H., Hausmann, S., Bang, W.Y., Ueda, A., Kondo, N., Hiraguri, A., Fukuhara, T., Bahk, J.D., Yun, D.J. and Bressan, R.A. (2004) *Arabidopsis* C-terminal domain phosphatase-like 1 and 2 are essential Ser-5-specific C-terminal domain phosphatases. *Proc. Natl Acad. Sci. USA* 101: 14539–14544.

Kuzmin, E.V., Karpova, O.V., Elthon, T.E. and Newton, K.J. (2004) Mitochondrial respiratory deficiencies signal up-regulation of genes for heat shock proteins. *J. Biol. Chem*. 279: 20672–20677.

Lee, Y.J., Kim, D.H., Kim, Y.W. and Hwang, I. (2001) Identification of a signal that distinguishes between the chloroplast outer envelope membrane and the endomembrane system in vivo. *Plant Cell* 13: 2175–2190.

Lüer, C., Schauer, S., Möbius, K., Schulze, J., Schubert, W.D., Heinz, D.W., Jahn, D. and Moser, J. (2005) Complex formation between glutamyl-tRNA reductase and glutamate-1-semialdehyde 2, 1-aminomutase in *Escherichia coli* during the initial reactions of porphyrin biosynthesis. *J. Biol. Chem*. 280: 18568–18572.

Matsumoto, F., Obayashi, T., Sasaki-Sekimoto, Y., Ohta, H., Takamiya, K. and Masuda, T. (2004) Gene expression profiling of the tetrapyrrole metabolic pathway in *Arabidopsis* with a mini-array system. *Plant Physiol*. 135: 2379–2391.

Moseley, J., Page, M., Alder, N., Eriksson, M., Quinn, J., Soto, F., Theg, S., Hippler, M. and Merchant, S. (2002) Reciprocal expression of two candidate di-iron enzymes affecting photosystem I and light-harvesting complex accumulation. *Plant Cell* 14: 673–688.

Moseley, J., Quinn, J., Eriksson, M. and Merchant, S. (2000) The Crd1 gene encodes a putative di-iron enzyme required for photosystem I accumulation in copper deficiency and hypoxia in *Chlamydomonas reinhardtii*. *EMBO J*. 19: 2139–2151.

Moser, J., Schubert, W.D., Beier, V., Bringemeier, I., Jahn, D. and Heinz, D.W. (2001) V-shaped structure of glutamyl-tRNA reductase, the first enzyme of tRNA-dependent tetrapyrrole biosynthesis. *EMBO J*. 20: 6583–6590.

Mukherjee, I., Campbell, N., Ash, J. and Connolly, E. (2006) Expression profiling of the Arabidopsis ferric chelate reductase (FRO)

gene family reveals differential regulation by iron and copper. *Planta* 223: 1178–1190.

Nagata, N., Tanaka, R. and Tanaka, A. (2007) The major route for chlorophyll synthesis includes [3,8-divinyl]-chlorophyllide a reduction in *Arabidopsis thaliana*. *Plant Cell Physiol*. 48: 1803–1808.

Nasrulhaq-Boyce, A., Griffiths, W. and Jones, O. (1987) The use of continuous assays to characterize the oxidative cyclase that synthesizes the chlorophyll isocyclic ring. *Biochem. J*. 243: 23–29.

Nogaj, L.A. and Beale, S.I. (2005) Physical and kinetic interactions between glutamyl-tRNA reductase and glutamate-1-semialdehyde aminotransferase of *Chlamydomonas reinhardtii*. *J. Biol. Chem*. 280: 24301–24307.

Nott, A., Jung, H.S., Koussevitzky, S. and Chory, J. (2006) Plastid-to-nucleus retrograde signaling. *Annu. Rev. Plant Biol*. 57: 739–759.

Pinta, V., Picaud, M., Reiss-Husson, F. and Astier, C. (2002) *Rubrivivax gelatinosus* acsF (previously orf358) codes for a conserved, putative binuclear-iron-cluster-containing protein involved in aerobic oxidative cyclization of Mg-protoporphyrin IX monomethylester. *J. Bacteriol*. 184: 746–753.

Pontier, D., Albrieux, C., Joyard, J., Lagrange, T. and Block, M.A. (2007) Knock-out of the magnesium protoporphyrin IX methyltransferase gene in *Arabidopsis*: effects on chloroplast development and on chloroplast-to-nucleus signaling. *J. Biol. Chem*. 282: 2297–2304.

Rzeznicka, K., Walker, C.J., Westergren, T., Kannangara, C.G., von Wettstein, D., Merchant, S., Gough, S.P. and Hansson, M. (2005) Xantha-l encodes a membrane subunit of the aerobic Mg-protoporphyrin IX monomethyl ester cyclase involved in chlorophyll biosynthesis. *Proc. Natl Acad. Sci. USA* 102: 5886–5891.

Sambrook, J. and Russell, D.W. (2001) Molecular Cloning: A Laboratory Manual. *In* . Cold Spring Harbor Laboratory Press, Cold Spring Harbor, NY.

Shepherd, M., McLean, S. and Hunter, C.N. (2005) Kinetic basis for linking the first two enzymes of chlorophyll biosynthesis. *FEBS J*. 272: 4532–4539.

Tanaka, R. and Tanaka, A. (2007) Tetrapyrrole biosynthesis in higher plants. *Annu. Rev. Plant Biol*. 58: 321–346.

Tottey, S., Block, M.A., Allen, M., Westergren, T., Albrieux, C., Scheller, H.V., Merchant, S. and Jensen, P.E. (2003) *Arabidopsis* CHL27, located in both envelope and thylakoid membranes, is required for the synthesis of protochlorophyllide. *Proc. Natl Acad. Sci. USA* 100: 16119–16124.

Wu, H., Li, L., Du, J., Yuan, Y., Cheng, X. and Ling, H.Q. (2005) Molecular and biochemical characterization of the Fe(III) chelate reductase gene family in *Arabidopsis thaliana*. *Plant Cell Physiol*. 46: 1505–1514.

Wu, Z., Zhang, X., He, B., Diao, L., Sheng, S., Wang, J., Guo, X., Su, N., Wang, L. and Jiang, L. (2007) A chlorophyll-deficient rice mutant with impaired chlorophyllide esterification in chlorophyll biosynthesis. *Plant Physiol*. 145: 29–40.

Zheng, C.C., Porat, R., Lu, P. and O'Neill, S.D. (1998) PNZIP is a novel mesophyll-specific cDNA that is regulated by phytochrome and a circadian rhythm and encodes a protein with a leucine zipper motif. *Plant Physiol*. 116: 27–35.

(Received June 14, 2008; Accepted July 30, 2008)